Microscope-based static light-scattering instrument

M. T. Valentine, A. K. Popp, and D. A. Weitz

Department of Physics and Division of Engineering and Applied Sciences, Harvard University, Cambridge, Massachusetts 02138

P. D. Kaplan

Unilever Research, Edgewater, New Jersey 07020

We describe a new design for a microscope-based static light-scattering instrument that provides simultaneous high-resolution images and static light-scattering data. By correlating real space images with scattering patterns, we can interpret measurements from heterogeneous samples, which we illustrate by using biological tissue. © 2001 Optical Society of America

OCIS codes: 180.0180, 290.0290, 100.2960, 170.6930, 170.3890, 170.4730.

Static light scattering (SLS) is a well-established technique for determining size, shape, and structure by measuring the intensity, $I(q)$, as a function of the scattering wave vector, q. In some cases, when there is independent information about the sample, the interpretation of $I(q)$ is straightforward; however, when little is known about the sample, the analysis can be more difficult. Measurement of $I(q)$ provides an ensemble average over the entire illumination volume, making the interpretation of scattering from highly heterogeneous samples particularly challenging. To facilitate the interpretation of SLS in these more-complex systems, we have designed a microscope-based light-scattering instrument that allows us to illuminate selectively a volume of interest while independently imaging the probed regions. Unlike several earlier implementations,[1–4] our design combines simultaneous high-resolution imaging with light scattering from well-defined volumes at well-defined wave vectors, permitting controlled placement of the illuminating beam, and correlation of scattering with visualized structures. With this instrument we probe the details of heterogeneous materials such as biological tissues.

Our design is based on a commercial inverted microscope (Leica DM-IRBE) and is shown schematically in Fig. 1. The source of the illumination is an Ar^+-ion laser (Coherent Innova 304) operating at a wavelength of $\lambda = 514.5$ nm *in vacuo*. The beam is launched from a fiber-optic coupler that is mechanically mounted above the condenser lens. A fraction of the beam is diverted onto a photodiode to monitor the intensity of the incident beam, and a series of neutral-density (N.D.) filters attenuates the laser intensity to typically less than 50 μW at the condenser entrance. The laser beam is focused to a point in the back focal plane (BFP) of a high-numerical-aperture oil-immersion condenser by a lens placed conjugate to the field iris. With the microscope in Koehler illumination, the condenser acts as a relay lens that reimages the collimated beam waist onto the sample, where the diameter of the excitation beam is smaller by an amount determined

by the magnification of the condenser. Typically, a 2-mm beam at the field iris is reduced to 80 μm in the sample, with a divergence of less than 10 mrad.

On the collection side of the sample, an oil-immersion objective lens (plan−apochromatic; 100× magnification; N.A., 1.4) collects the scattered light and transmitted beam. We reimage the scattered light to an intermediate plane conjugate to the BPF of the objective, using a custom-made (Leica) projection system positioned above the camera port of the trinocular head of the microscope. Into this plane we insert a beam block mounted upon an $x-y$ translation stage and
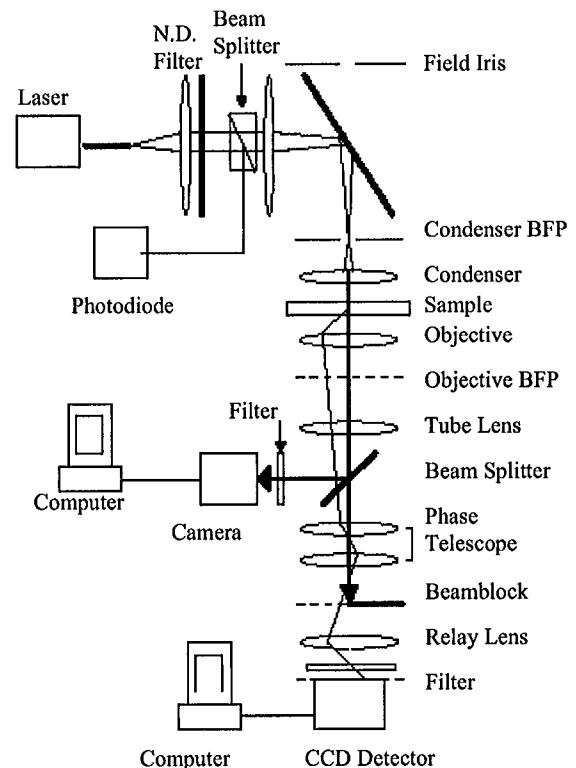

Fig. 1. Schematic of the optical arrangement of the SLS microscope.

manually aligned for each measurement. A final relay lens reimages the intermediate scattering plane onto a cooled CCD detector (Princeton Instruments Model CCD-512 SF) with a 512×512 array of $24 \ \mu$m $\times 24 \ \mu$m pixels and a 16-bit dynamic range. The real space image of the sample is simultaneously obtained by video camera (Hitachi KP-M1U) at the side port of the microscope.

Unlike two-dimensional spatial Fourier transforms of real-space images, the scattering patterns measured with the static light-scattering microscope are full three-dimensional transforms that ensure ensemble averaging over the entire illuminated volume; this is essential for correct capture of the bulk properties of localized regions of heterogeneous samples. The collection optics can be modified to perform dynamic light-scattering measurements[5] in addition to SLS; standard microscopy techniques are also available.

Quantitative measurements require several calibrations. First, we determine how scattering wave vectors map onto the CCD detector. In the BPF of the objective, the radial distance of the scattered light from the transmitted beam, δx, is directly proportional to the sine of the scattering angle, θ. However, at the detector we measure a nonlinear relationship that is due to image-deforming optical aberrations caused by the relay lens. We measure this relationship by scattering from a graticule imprinted upon a glass slide and measuring the positions of several orders m of diffraction peaks. Using Bragg's law, we calculate the corresponding scattering angles: $\sin \theta = m\lambda/n_G d$, where d is the graticule spacing and n_G is the index of refraction of glass. We plot $\sin \theta$ as a function of δx, fit a third-order polynomial to the resultant data, and apply this expression to any sample with known refractive index n_S to calculate the scattering wave vector, $q = (4\pi n_s/\lambda)\sin\{1/2 \arcsin[(n_G/n_s)\sin(\theta)]\}$.

There are also several calibrations for the CCD detector that must be performed to account properly for variations in pixel sensitivity, stray light, dark counts, pixel readout noise, and any offset in the black-level reference voltage of the camera.[6] To measure dark counts caused by thermal electrons we remove the detector from the microscope and place it in a light-tight box to obtain a dark image at each exposure time. To perform a flat-field correction for nonuniformities in pixel sensitivity we uniformly illuminate the detector and obtain a background image in which any gradients in the contrast arise only from variations in pixel response and normalize this background image by dividing by the mean illumination intensity. We calculate corrected images by subtracting the dark image and dividing by the flat-field background image. Finally, to reduce the effects of small angle flare, we correct the signal obtained by scattering from a solvent-filled sample chamber as above and subtract it from the corrected image obtained from the sample for every measurement; in the case of the tissue samples, an empty sample chamber is used.

To test the apparatus experimentally, we measure $I(q)$ for a dilute suspension of 2.0-μm-diameter latex spheres (Interfacial Dynamics Corporation) in water. In the dilute limit, the measured $I(q)$ is $F(q)$, where

$F(q)$ is the form factor of a single sphere. As shown in Fig. 2, the results compare quite well with the predictions of Mie scattering theory,[7] as shown by the solid curve. At large wave vectors, however, optical aberrations prevent the formation of a clear image, precluding determination of the fine details in the form factor. This is a purely optical effect that can be corrected by a more-sophisticated system of relay optics. The utility of simultaneous imaging and scattering is demonstrated in Figs. 3A and 3B, where we show images and corresponding scattering patterns from a partially ordered two-dimensional packing of the latex spheres. Strong local orientational ordering results in
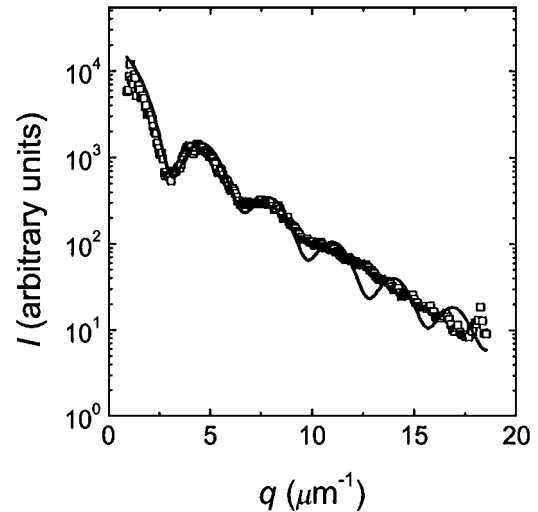
Fig. 2. $I(q)$ measured from a dilute suspension of 2.0-μm spheres in a 1:1 mixture of $H_2O:D_2O$ at $\phi = 10^{-3}$. Solid curve, form factor predicted from Mie theory with no fitting parameters.
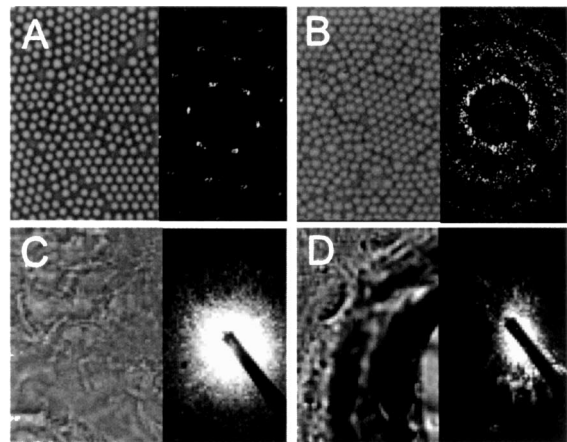
Fig. 3. A, B, Real-space and scattering-space images from a monolayer of 2.0-μm particles: A, a region with one dominant crystal orientation, resulting in pronounced Bragg peaks; B, regions with polycrystalline domains, resulting in a Bragg ring and indicating the average nearest-neighbor distance, $2.00 \pm 0.04 \ \mu$m. C, D, Real-space and scattering-space images from porcine skin tissue: C, The real-space image shows a region devoid of any large heterogeneities; the resultant scattering pattern is isotropic. D, A region from the same slice in the vicinity of a hair, resulting in an anisotropic scattering pattern.

well-defined Bragg spots (Fig. 3A), whereas local polycrystallinity results in a Bragg ring (Fig. 3B); this demonstrates the sensitivity of light scattering to even small changes in organization or symmetry.

This instrument's strength is its ability to facilitate local light-scattering measurements on heterogeneous samples, which is particularly important for biological materials that include many small structures with a wide range of shapes and orientations. To illustrate this property we measure the scattering from thin slices of porcine skin tissue,[8] for which the microscopic origins of light scattering are poorly understood. The nature of light propagation through tissue has important implications for medical applications such as laser surgery, optical biopsy, photodynamic therapy, and laser treatment dosimetry.[9–11] Whereas considerable effort has focused on measuring average absorption and scattering coefficients,[12,13] little attention has been given to the effects of small yet abundant heterogeneities on bulk scattering properties in tissue.

We use a cryomicrotome to slice porcine skin tissue into approximately 20-μm-thick slices, with total surface area of typically 1 cm^2, and set the laser beam diameter to $70-100$ μm. We find that in the dermis, where individual cells are separated by large regions of extracellular matrix, large-scale structural heterogeneities, such as acellular voids, hairs or hair follicles, and pigments, can cause dramatic changes in the scattering patterns. In Figs. 3C and 3D we show the real space and the scattering-space images from a typical experiment. Figure 3C shows a region devoid of any large heterogeneities; the resultant scattering pattern is isotropic. Figure 3D shows a region from the same slice of tissue near the vicinity of a hair. The scattering pattern is anisotropic and shows more structure than the homogeneous case. These results suggest that models that do not incorporate details of local tissue microstructure may not capture the anisotropic features of the scattering patterns.[14–16] Because light can be dramatically redirected in the vicinity of a structure, improved models are necessary for prediction of local radiation dosage and improvement of the precision of medical laser treatments to small regions of heterogeneous tissue. These improved models must correctly capture the effects of anisotropy, demonstrated in Fig. 3D; this can conveniently be done through concurrent analysis of both the radial and the azimuthal dependences of the scattering. For example, a Fourier analysis of the azimuthal dependence of the scattering will directly identify the nature of the anisotropy and will permit rapid and convenient identification of specific features.

The static scattering microscope is sensitive to local structure in complex systems. It can detect variations in structure and organization in thin tissue samples, making it potentially useful for pathohistological studies. Further development of analysis techniques to parameterize the scattering patterns may permit the application of local light-scattering measurements to the automated classification of cellular phenotype and to the identification of diseased tissue that is characterized by changes in size, shape, or organization.

References

1. I. Nishio, T. Tanaka, S.-T. Sun, Y. Imanishi, and S. T. Ohnishi, Science **220,** 1173 (1983).
2. T. Nishizaki, T. Yagi, Y. Tanaka, and S. Ishiwata, Nature **361,** 269 (1993).
3. D. E. Burger, J. H. Jett, and P. F. Mullaney, Proc. SPIE **190,** 467 (1979).
4. P. S. Blank, R. B. Tishler, and F. D. Carlson, Appl. Opt. **26,** 351 (1987).
5. P. D. Kaplan, V. Trappe, and D. A. Weitz, Appl. Opt. **38,** 4151 (1999).
6. S. Inoue and K. R. Spring, *Video Microscopy: The Fundamentals* (Plenum, New York, 1997).
7. H. C. van de Hulst, *Light Scattering by Small Particles* (Dover, New York, 1981).
8. A. K. Popp, M. T. Valentine, P. D. Kaplan, and D. A. Weitz, Proc. SPIE **3917,** 22 (2000).
9. J. B. Fishkin, O. Coquoz, E. R. Anderson, M. Brenner, and B. J. Tromberg, Appl. Opt. **36,** 10 (1997).
10. G. J. Tearney, M. E. Brezinski, and J. G. Fujimoto, Science **276,** 2037 (1997).
11. J. R. Mourant, I. J. Bigio, J. Boyer, R. L. Conn, T. Johnson, and T. Shimada, Lasers Surg. Med. **17,** 350 (1995).
12. B. Beauvoit and B. Chance, Mol. Cell. Biochem. **184,** 445 (1998).
13. S. J. Matcher, M. Cope, and D. T. Delpy, Appl. Opt. **36,** 386 (1997).
14. A. H. Hielscher, R. E. Alcouffe, and R. L. Barbour, Phys. Med. Biol. **43,** 1285 (1998).
15. B. C. Wilson and G. Adam, Med. Phys. **10,** 824 (1983).
16. I. S. Saidi, S. L. Jacques, and F. K. Tittel, Appl. Opt. **34,** 7410 (1995).